Journal of the European Ceramic Society 19 (1999) 2257–2264

PII: S0955-2219(99)00108-9
0955-2219/99/$ - see front matter

Parallel Molecular Dynamics Simulations of High Temperature Ceramics

Alok Chatterjee, [a]* Timothy Campbell, [a] Rajiv K. Kalia, [a] Aiichiro Nakano, [a] Andrey Omeltchenko, [a] Kenji Tsuruta, [a] Priya Vashishta [a] and Shuji Ogata [b]

[a]Concurrent Computing Laboratory for Materials Simulations, Department of Physics and Astronomy, Department of Computer Science, Louisiana State University, Baton Rouge, LA 70803, USA
[b]Department of Applied Sciences, Yamaguchi University, 2557 Tokiwadai, Ube 755-8611, Japan

Abstract

'Grand Challenge' atomistic simulations of high-temperature structural materials are performed on multiple, parallel platforms. The simulations focus on sintering of ceramic nanoclusters, structure and mechanical properties of nanophase ceramics, and hypervelocity impact damage in diamond coatings. © *1999 Elsevier Science Ltd. All rights reserved.*

Keywords: diamond, molecular dynamics, nanophase, fracture, Si_3N_4.

1 Introduction

Novel materials that can withstand high temperatures and extreme environments are generating considerable worldwide attention. Such materials are tremendously important for defense and civilian technologies. The basic requirements for designing materials that have low densities, elevated melting temperatures, high oxidation and corrosion resistance, the ability to resist creep, and high toughness encompass some of the most challenging problems in materials science. Despite a great deal of experimental research, many perplexing problems remain concerning mechanical properties and thermal behavior of high-temperature materials (HTMs). With the recent emergence of highly efficient multiresolution algorithms and massively parallel machines, materials simulation has reached a level of sophistication that can aid experimental efforts involved in the synthesis of novel HTMs.

We have performed 'Grand Challenge' atomistic simulations of high-temperature structural materials on multiple, parallel platforms. The simulations have focused on sintering of ceramic nanoclusters, structure and mechanical properties of nanophase ceramics, and hypervelocity impact damage in diamond coatings. In the next section, we describe the multiscale algorithms and parallel implementation of molecular-dynamics (MD) simulations. Sections 3, 4 and 5 describe the results of large-scale parallel MD simulations of Si_3N_4 nanoclusters, nanophase Si_3N_4, and diamond coatings respectively. Section 6 contains a summary of future directions of research in HTMs.

*To whom correspondence should be addressed now with: IPNS, Argonne National Laboratory, Argonne, IL, USA; e-mail: achatterjee@anl.gov

2 Parallel Molecular-Dynamics Simulations

Atomistic simulations discussed below require considerable computational resources because of long processing times, large systems, and compute-intensive interatomic interactions (e.g. long-range Coulomb and three-body covalent forces). These simulations are not feasible without efficient algorithms and massively parallel machines.

We have designed a highly efficient, multiresolution molecular-dynamics (MRMD) approach to carry out large-scale materials simulations on parallel machines.[1] This approach includes the fast multipole method (FMM)[2]—a divide-and-conquer scheme which reduces the computational cost for the Coulomb interaction from $O(N^2)$ to $O(N)$. The FMM is based on a hierarchical subdivision of space (Fig. 1 left), where at each spatial scale the influence of a large collection of charges is approximated to any desired precision by a multipole expansion. The method is well-suited to parallel architectures: unlike the direct method which must communicate the locations and strengths of a large number of charges between distant processors, the FMM transmits a compressed representation of this information, namely the coefficients of the multipole expansion. In addition to FMM, the MRMD approach includes a multiple time-scale algorithm[3] for short-ranged, two-body interactions and a separable scheme for three-body covalent interactions.

Figure 1 (right) shows the performance of the MRMD approach[1] on the 512-node Touchstone Delta machine at Caltech and the 128-processor IBM SP system at Argonne National Laboratory. The execution time scales linearly with the system size and the computation time dominates the communication time. Using MPI (Message Passing Interface), the MRMD has been ported to other parallel platforms as well.

In many atomistic simulations (e.g. porous materials or fracture) one encounters a non-uniform spatial distribution of atoms. Regular partitioning of such a system into subsystems of equal volume and then one-to-one mapping of subsystems on processors of a parallel machine leads to an imbalance of the computational workload among the processors. We have developed a load-balancing algorithm with a small runtime overhead.[4] The algorithm is based on a novel concept that the computational space shrinks in the region where the workload density is high so that the load is uniformly distributed. This is achieved by introducing a curvilinear coordinate transformation, $\xi = x + u(x)$. Workloads are partitioned with a uniform 3-dimensional mesh in the curvilinear coordinate system, ξ [Fig. 2(a)]. This leads to curved partition boundaries in the Euclidean space, x, and the load-imbalance and communication costs are minimized as a functional of $u(x)$. Simulated annealing (SA) technique is used to solve this minimization problem. We find that a multiresolution analysis based on wavelets leads to a compact representation of $u(x)$, and accordingly to fast convergence of the minimization procedure.

The new load-balancer is highly scalable: for a $1{\cdot}04\times10^9$ atom MD simulation on 64 IBM SP2 nodes, the parallel efficiency is 0·92 [Fig. 2(b)]. The load-balancer is also light-weight: accounting for only 4·5% of the total execution time of the MD program (repartitioning with 5 SA iterations is done every 60 MD steps).

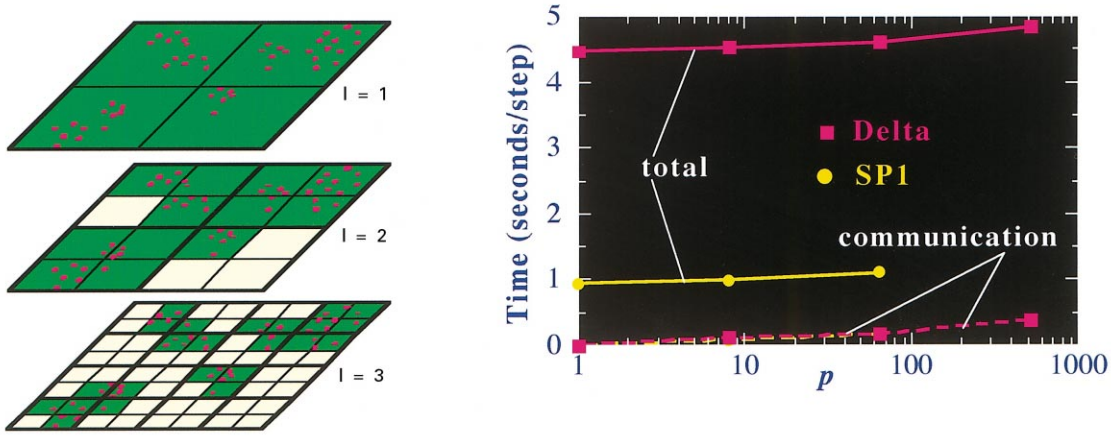

Fig. 1. (Left) multilevel FMM decomposition for a 2-D system. (Right) execution (solid curves) and communication times (dashed curves) per MD time step for the MRMD approach; p is the number of processors.

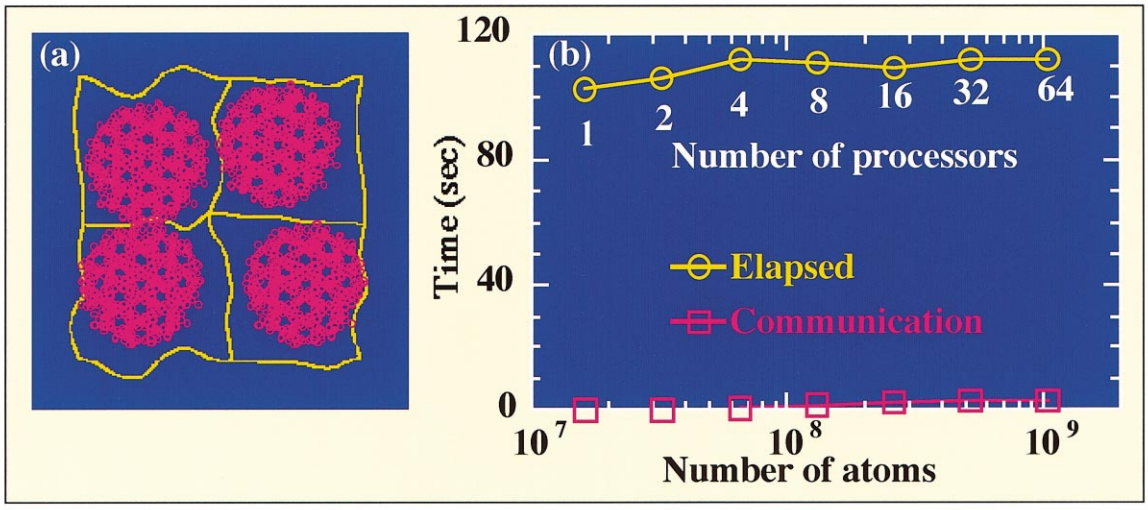

Fig. 2. (a) 2-D slice of a curvilinear partition in Euclidean space. (b) Performance of the adaptive curvilinear-coordinate load-balancer on 64 IBM SP2 nodes. Each node has $16{\cdot}25\times10^6$ atoms. Note the increase in the execution time is only 10% even though the size of the system increases from $16{\cdot}25\times10^6$ to $1{\cdot}04\times10^9$ atoms.

3 Sintering of Silicon Nitride Nanoclusters

The study of structural and mechanical properties of nanophase Si_3N_4 was preceded by MD simulations of sintering of silicon nitride nanoclusters (each cluster consisted of 20,335 atoms).[5] Our MD calculations provide a microscopic view of neck formation during early stages of sintering at 1730°C (Fig. 3). Initially, there is significant motion of clusters with respect to each other. This is followed by bonding between the two nanocrystals through Si and N atoms. For 100 ps, the two bounded nanocrystals rotate relative to each other. Subsequently, over the next 100 ps the relative motion damps out while an asymmetric neck begins to form between the two nanocrystals. The neck region is populated by four-fold and to a lesser extent three-fold coordinated Si atoms. In a similar fashion, we have investigated the sintering of amorphous silicon nitride nanoclusters at 1730°C. Amorphous nanoclusters form a symmetric neck and the neck region between amorphous nanoclusters has nearly the same number of three- and four-fold coordinated Si atoms. For both nanocrystals and amorphous nanoclusters, sintering is driven by diffusion of surface atoms. The diffusion in the neck region of amorphous clusters is four times faster than in the neck between nanocrystals.

4 Structure and Mechanical Properties of Nanophase Si_3N_4

Advanced ceramics such as Si_3N_4, SiC, SiO_2, and Al_2O_3 are highly desirable materials for applications requiring extreme operating conditions. Light weight, elevated melting temperatures, high strengths, and wear and corrosion resistance make them very attractive for applications in aeronautics, automotive, electronics, and advanced manufacturing industries. The only serious drawback of ceramics is that they are brittle at low to moderately high temperatures.

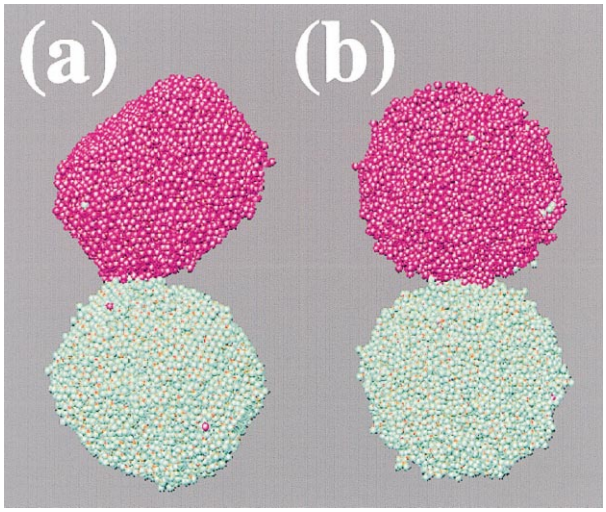

Fig. 3. Snapshots showing sintering of Si_3N_4 nanoclusters at 1730°C: (a) sintered nanocrystals at $t = 200$ ps; and (b) sintered amorphous nanoclusters at $t = 400$ ps.

In recent years it has become possible to fabricate 'ductile' ceramics and harder metals by consolidation of nanometer size clusters; these are known as nanophase materials. The key issues concerning structure and physical properties of these novel nanophase materials remain unanswered. Experiments have yet to provide information regarding the morphology of pores or the structure and dynamics of atoms in nanophase materials. In the field of modeling only a few atomistic simulations of nanophase materials have been reported thus far. (Simulations of nanophase materials are computationally very demanding: since each nanocluster itself consists of 10^3–10^4 atoms they require $\sim 10^6$ atoms and 10^5–10^6 time steps for processing.)

Using $1{\cdot}08 \times 10^6$ particle MD simulations we have investigated the structure and mechanical behavior of nanophase Si_3N_4.[6–8] Effective two- and three-body interatomic potentials are used in the MD simulations. The two-body terms consist of steric repulsion between atoms, screened Coulomb potentials due to charge transfer between Si and N, and a charge-dipole interaction that takes into account the large electronic polarizability of nitrogen; the three-body potential in Si_3N_4 takes into account covalent effects through bond-bending and bond-stretching terms. The potential is validated by comparing the MD results with experimental measurements. The comparison shows that: (i) the bond lengths and bond-angle distributions in crystalline and amorphous Si_3N_4 are in excellent agreement with experiments;[9] (ii) the positions and relative heights of the peaks in the static structure factor for amorphous Si_3N_4 are in good agreement with neutron scattering measurements; (iii) the vibrational density-of-states of crystalline α-Si_3N_4 agrees well with inelastic neutron scattering experiments; (iv) the specific heat of crystalline α-Si_3N_4 is in excellent agreement with experiments over a wide range of temperatures; and (v) the elastic moduli along different directions of α-Si_3N_4 deviate less than 10% from the experimental values.

We create nanophase Si_3N_4 by generating nanoclusters and consolidating a random configuration (108 clusters with 10,052 atoms each) of these clusters with the constant-pressure MD approach. Structural analyses (pair-distribution functions and bond-angle distributions) indicate

that interfacial regions are amorphous with a large number of undercoordinated Si atoms. We have investigated the morphology of pores during the sintering process and also the dependence of elastic moduli on porosity and grain size. The variation of elastic moduli on porosity can be understood in terms of a three-phase model for heterogeneous materials (see Fig. 4).[7]

Using $1{\cdot}08\times10^6$ particle MD simulations, we have investigated the morphological and dynamic aspects of fracture in nanophase Si_3N_4.[8] Snapshots of the crack front at various values of the external strain are shown in Fig. 5. The crack front includes pores connected to the notch (shown in red; the remaining disconnected pores are shown in yellow). Figure 5(a) shows a crack-front snapshot taken 10 ps after the notch is inserted. We observe slight propagation of the crack front and the growth of a few crack branches in the system. These local branches and nanoclusters tend to arrest the motion of the primary crack front, and further crack propagation is seen when the applied strain is increased. At 11% strain the crack front has advanced significantly through coalescence with pores in the center. Pores and interfacial regions allow the crack front to meander and form a branched structure. Figure 5(b) shows the crack-front and other pores in the system 10 ps after the system was strained to 14%. At this time a secondary crack (top left-hand corner of the figure) with several local branches merges with the primary crack. Further increase in the strain causes the secondary front to advance toward the initial notch while the crack keeps growing laterally. At a strain of 30%, the material is separated into two disconnected parts. It should be noted that the fracture strain (30%) is an order-of-magnitude larger than that at which the crystalline Si_3N_4 system fractures. In the nanophase system, the fracture is caused by: (i) plastic deformation in interfacial regions; (ii) deflection and arrest of cracks by nanoclusters; and (iii) multiple crack branching. In contrast, the fracture is cleavage-like in the crystalline system. This demonstrates the dramatic effect of nanostructures on fracture.

Crack-front morphology has become a significant issue in recent years. Measurements of widths of fracture profiles in a variety of brittle and ductile solids reveal that it scales with the lengths as $w\sim L\zeta$. For out-of-plane fracture profiles, the roughness exponent, $\zeta_\perp$, has a value of 0·8 in three and 0·7 in two spatial dimensions above a certain length scale. These values of $\zeta_\perp$, are found to be independent of the material or the mode of fracture.[10] At small length scales or when the crack-front propagates quasi-statically, the roughness exponent crosses over to a smaller value $\sim$0·5. Recently, it has also be pointed out that roughness exponent for in-plane fracture profiles is $\sim$0·6.

We have determined roughness exponents for fracture surfaces in nanophase Si_3N_4, by calculating the height-height correlation functions both in and out of the fracture plane y-z. Figure 6 shows that the out-of-plane fracture profile perpendicular to the crack propagation has two roughness exponents: $\zeta = 0{\cdot}84 \pm 0{\cdot}12$ above a certain length scale (64 Å) and $\zeta = 0{\cdot}58 \pm 0{\cdot}14$ otherwise. For the other out-of-plane height-height correlation function

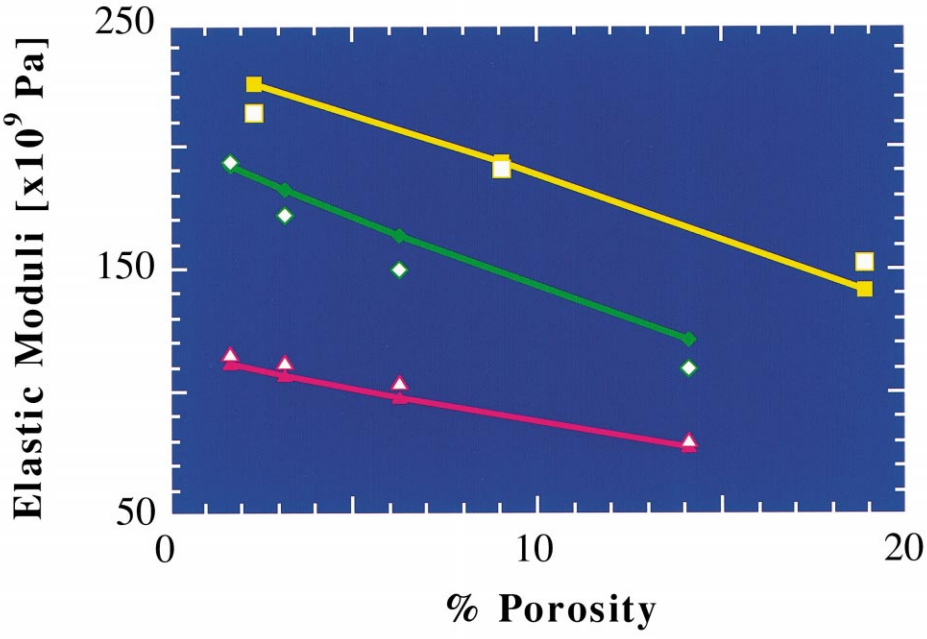

Fig. 4. Porosity dependence of the bulk modulus (K) and shear modulus (G). Open squares denote the MD results for bulk moduli of nanophase silicon nitride with cluster size $D = 60$ Å; open diamonds and triangles represent the MD results for bulk and shear moduli, respectively, of the nanophase system with 45 Å clusters. Solid squares and diamonds denote bulk moduli and solid triangles represent shear moduli calculated from the multicomponent model. The solid lines are drawn as a guide to the eye.

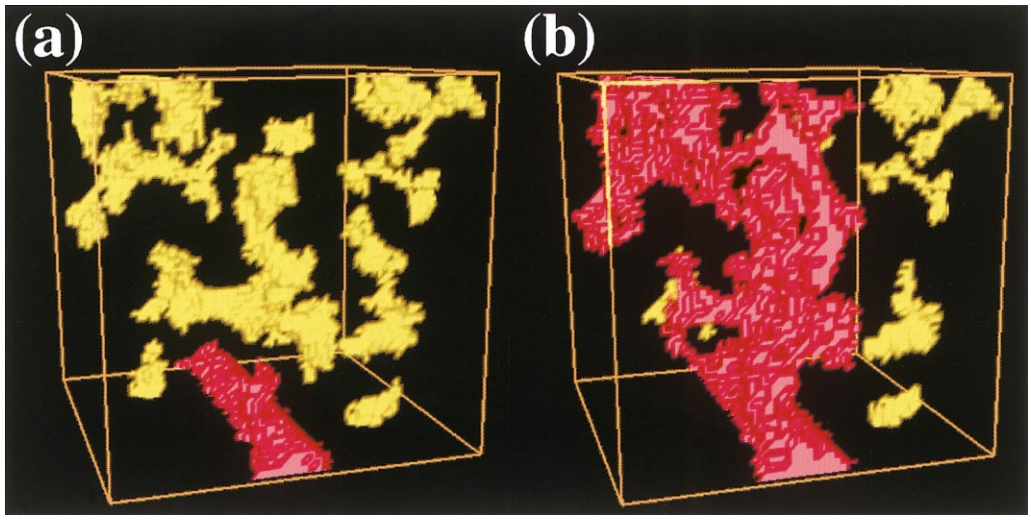

Fig. 5. Snapshots of the crack front (shown in red) along with large ($>6{\cdot}4$ nm^3) isolated pores (shown in yellow) in the strained nanophase system: (a) initial notch with crack branches and pores in the system under an applied strain of 5%; (b) the primary and secondary crack fronts at 14% strain on the system.

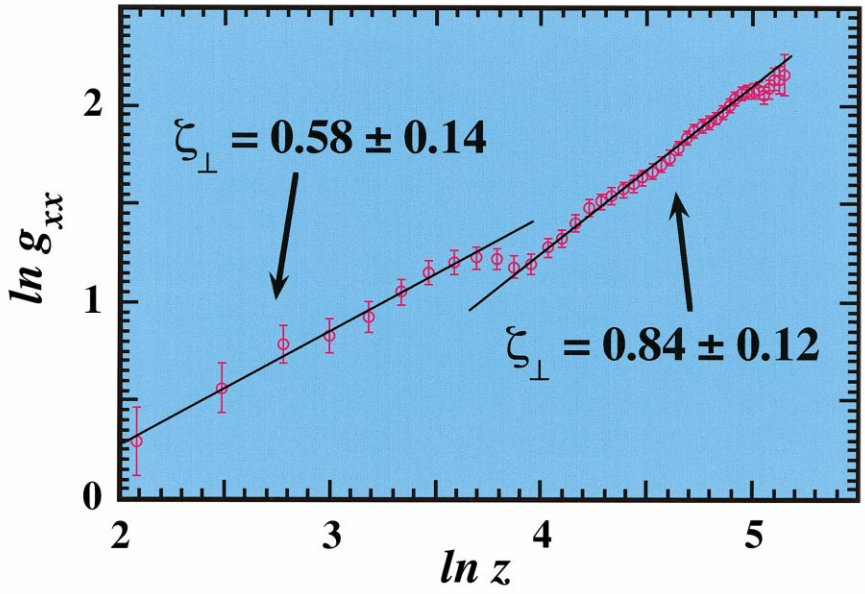

Fig. 6. Plot of $\ln g_{xx}(z)$, the log of the height–height correlation function perpendicular to the direction of crack propagation, versus $\ln(z)$ for the out-of-plane fracture profile. Two roughness exponents are observed for different length scales.

(parallel to the crack propagation) we find the roughness exponent to be $0{\cdot}75 \pm 0{\cdot}08$. The in-plane fracture profile for nanophase Si_3N_4 is found to be $0{\cdot}57 \pm 0{\cdot}08$. Similar results have been found experimentally in Al–Li and super α_2 Ti_3Al-based alloys.

5 Hypervelocity Impact Damage in a Diamond Coating

Damage resulting from debris impact in low earth orbit (LEO) presents a major consideration for materials in space applications. Numerous laboratory experiments have been performed to simulate these phenomena. In an attempt to simulate such debris-impact experiments on parallel computers, we have performed large-scale MD calculations to determine the hypervelocity impact damage caused by a diamond crystallite on a diamond coating. (Rocketdyne in collaboration with Phillips Laboratory are using chemical vapor deposition to apply thin films of diamond to surfaces for a wide range of rocket applications.) The MD simulations are based on a reactive bond order (REBO) potential proposed by Brenner *et al.*[11] This potential is quite unique in that it treats covalent bonding in molecular and solid-state structures with a single classical expression. Moreover, the potential can describe chemical processes such as covalent bond formation and breaking. The parameters of the potential have been fitted to experimental

values and first-principles calculations of bond lengths, bond energies, and force constants for several solid-state and molecular systems. The REBO potential has been shown to provide a good description of various properties outside the fitting database such as elastic constants and vibrational spectra of diamond and in-plane elastic properties of graphite. The results for the surface reconstruction and energetics of point defects in diamond are also in good agreement with experiments and electronic-structure calculations. The calculated formation energies for an extensive set of hydrocarbon molecules agree well with experimental results.

We have performed three hypervelocity impact-damage simulations (Fig. 7). In the first case the crystallite strikes the diamond film with a velocity of 8 km s^{-1}. The crystallite penetrates the film to a depth of 20 Å, causing the diamond structure of the film to graphitize without any crater formation. Subsequently the nearly-intact crystallite emerges from the coating at a speed of 4 km s^{-1}. In the second simulation the incoming crystallite strikes the coating at a speed of 11 km s^{-1}. Part of the crystallite disintegrates after impact, and almost all of its kinetic energy is imparted to the coating. In this case we observe the formation of a crater along with amorphization in the impact region. In the third case the crystallite hits the diamond coating at a velocity of 15 km s^{-1}. Unlike the first two cases, the crystallite completely disintegrates causing extensive damage including the creation of a crater.

6 Future Directions: Atomistic Processes in Alumina and Silicon Carbide

Silicon carbide and alumina are excellent structural ceramics for applications requiring extreme operating conditions. We are investigating dynamic fracture in SiC and the properties and processes in nanophase SiC (n-SiC) using large-scale MD simulations. The total interatomic potential for SiC is validated by checking the self-consistency of the MD results against structural and dynamical properties from experiments, including the lattice constant, cohesive energy, elastic moduli (c_{11}, c_{12}, c_{44}), bulk modulus and the phonon density-of-states. Figure 8 (left) shows a snapshot of a 10^6 atom MD simulation of fracture in crystalline SiC. By magnifying the crack tip region (inset) we can see the bond-breakage and local deformation indicating the onset of fracture. Recently, we have performed an extensive study of n-SiC through a combination of experimental and computational approaches. MD simulations and neutron scattering results indicate a substantial reduction in the sintering temperature (~1350°C) in the case of nanocluster assembled

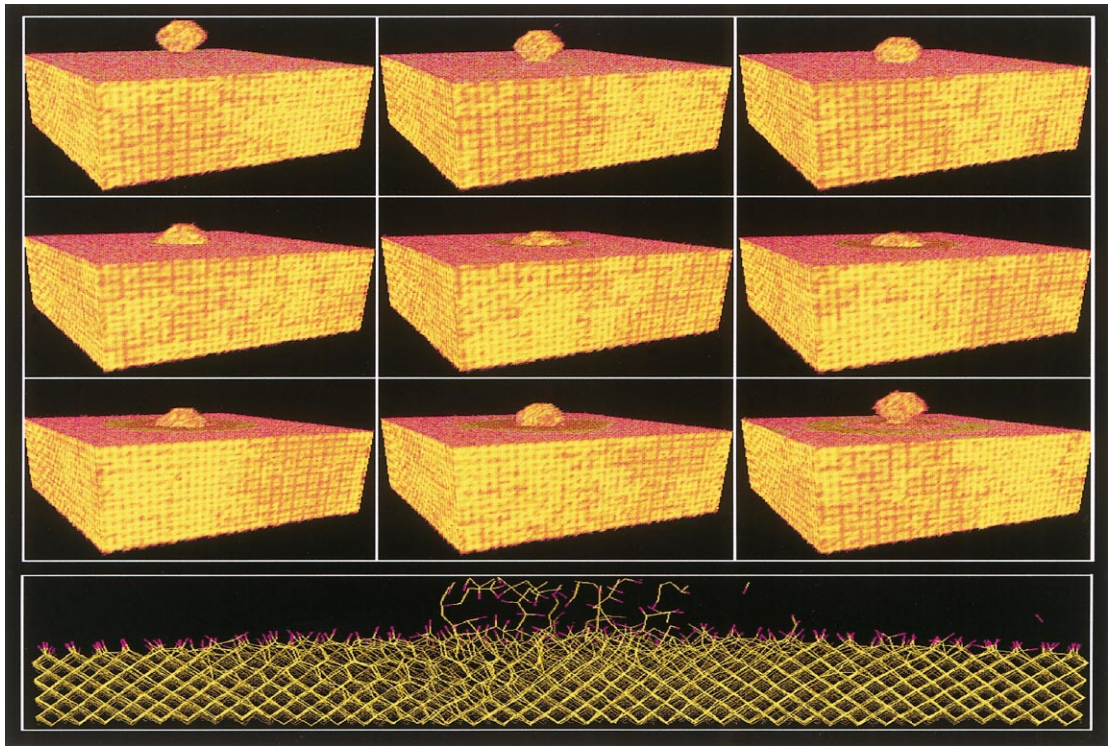

Fig. 7. The first nine snapshots (left to right) show the impact of a diamond crystallite (speed of 8 km s^{-1}) on a diamond coating. These MD simulations span a time period of 28 p. Upon impact, the crystallite penetrates the coating and then bounces out at a speed of 4 km s^{-1}. The last snapshot shows that the energy imparted to the coating causes graphitization under the contact region.

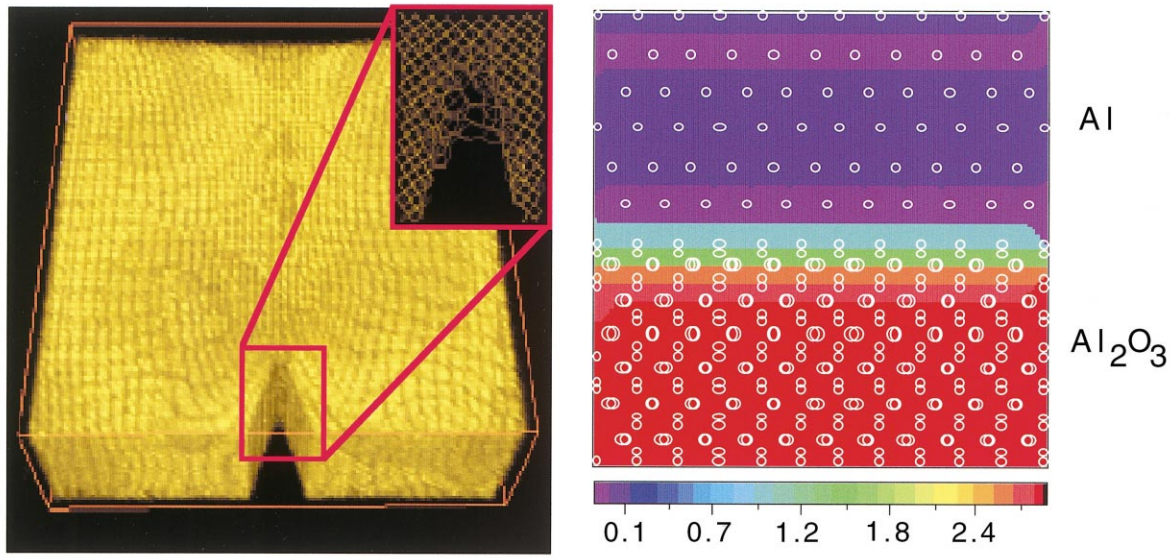

Fig. 8. The figure on the left shows the onset of fracture in a 10^6 atom MD simulation of crystalline SiC under 7% strain at room temperature. The other figure (right) shows dynamic charge transfer at Al/Al_2O_3 interface. The interface involves (111) Al and (0001) Al_2O_3 surfaces. The white circles show the atomic positions (the small circle is aluminum and the large circle is oxygen). The color bar shows the valence of the aluminum atoms.

SiC as compared to their coarse-grained counterparts (~1900–2100°C). The mechanism of sintering, at least in the early stages, is due to surface diffusion of atoms. The scaling exponents indicate that the average fractal dimension and roughness exponent for the nanophase system at different densities remain around 2 and 0·45 respectively. Structural analyses reveal amorphous interfacial regions in n-SiC. The observed elastic moduli in the nanophase SiC system decline substantially with an increase in the porosity of the system.[12]

The MD simulations for aluminum oxide are based on an interaction scheme proposed by Streitz and Mintmire.[13] This potential allows the local atomic charges to vary with the environment. The dynamic charge transfer and the resulting electrostatic potential is merged with an embedded-atom potential yielding an interaction scheme which can simultaneously treat fcc aluminum and α-alumina systems. This potential has been optimized to reproduce the bulk structural and mechanical properties of fcc aluminum and α-alumina. Additionally, the potential yields reasonable values for the surface energies and surface relaxations. We are currently investigating dynamic fracture in alumina, the aluminum/alumina interface, the oxidation of aluminum nanoclusters, and nanostructured aluminum/alumina composites. Figure 8 (right) shows a MD simulation of the aluminum/alumina interface; the color shows the valence of the aluminum atoms. We see that significant charge transfer occurs in the interface region thus reinforcing the necessity of including dynamic charge transfer in the MD simulations. Nanostructured composites made by consolidating passivated metal clusters are known to have many novel properties. Issues important to understanding the thermo-mechanical behavior of these nanostructured composites are the dynamics of the oxidation process, the structure and thickness of the passivation layer, and the stresses in the surface oxide. We have performed 10^6 atom MD simulations of the oxidation of nanometer size aluminum clusters. In MD simulations of the oxidation of a 20 nm aluminum cluster we find that an amorphous oxide of 40 Å thickness is formed; this is in good agreement with experimental results. Analyses of the surface-oxide reveal significant charge transfer in the oxide region and a variation of local structures when passing through the oxide from the metal-oxide interface to the oxide-environment interface.[14]

Acknowledgements

This work was supported by DOE (Grant No. DE-FG05-92ER45477), NSF (DMR-9412965, GER93550007, ASC-9701504), AFOSR (F 49620-94-1-0444), USC-LSU Multidisciplinary University Research Initiative (F 49620-95-1-0452), Army Research Office (DAAH04-96-1-0393), Petroleum Research Fund (31659-AC9), NASA (NAG2-1248, NAG2-1212), and Louisiana Education Quality Support Fund (LEQSF) (LEQSF(96-99)-RD-A-10). Simulations were performed on the IBM SP2 computer at the Maui High Performance Computing Center (MHPCC), the Hewlett–Packard/Convex Exemplar machine at the Center for Advanced Computing Research at Caltech, the IBM SP3 computer at Argonne National Laboratory, and

IBM SP, Cray T3E, and Silicon Graphics Origin 2000 machines at DoD's Major Shared Resource Centers (MSRC) through a DoD Challenge Award. Computations were also performed on parallel architectures at the Concurrent Computing Laboratory for Materials Simulations (CCLMS) at Louisiana State University. The facilities in the CCLMS were acquired with the Equipment Enhancement Grants from the LEQSF.

References

1. Kalia, R. K., de Leeuw, S. W., Nakano, A. and Vashishta, P. *Comput. Phys. Commun.*, 1993, **74**, 316; Nakano, A., Kalia, R. K., Vashishta, P., *Comput. Phys. Commun.*, 1994, **84**, 197.
2. Greengard, L. and Rokhlin, W., *J. Comput. Phys.*, 1987, **73**, 523.
3. Tuckerman, M. and Berne, B. J., *J. Chem. Phys.*, 1992, **97**, 1990.
4. Nakano, A. and Campbell, T., *T. Par. Comput.*, 1997, **23**, 1461.
5. Tsuruta, K., Omeltchenko, A., Kalia, R. K. and Vashishta, P., *Europhys. Lett.*, 1996, **33**, 441.
6. Tsuruta, K., Nakano, A., Kalia, R. K. and Vashishta, P., *J. Am. Ceram. Soc.*, 433, **81**, 1998.
7. Kalia, R. K., Nakano, A., Tsuruta, K. and Vashishta, P., *P. Phys. Rev. Lett.*, 1997, **78**, 689.
8. Kalia, R. K., Nakano, A., Omeltchenko, A., Tsuruta, K. and Vashishta, P., *Phys. Rev. Lett.*, 1997, **78**, 2144.
9. Vashishta, P., Kalia, R. K. and Ebbsjö, I., *Phys. Rev. Lett.*, 1995, **75**, 858.
10. Bouchaud, E. and Navéos, S., *J. Phys. I France*, 1995, **5**, 547.
11. Brenner, D. W., *Phys. Rev. B*, 1990, **42**, 9458; Sinnott, S. B., Colton, R. J. and Brenner, D. W., *Surf. Sci.*, 1994, **316**, 1055.
12. Chatterjee, A., Kalia, R. K., Loong, C.-K., Nakano, A., Omeltchenko, A., Tsuruta, K., Vashishta, P. and Winterer, M., to be published.
13. Streitz, F. H. and Mintmire, J. W., *Thin Solid Films*, 1994, **253**, 179; *Phys. Rev. B*, 1994, **50**, 11996.
14. Campbell, T., Kalia, R. K., Nakano, A., Vashishta, P., Ogata, S. and Rodgers, S., *Phys. Rev. Lett.*, 1999, **82**, 4866.